Geochemistry, Geophysics, Geosystems®

AGU ADVANCING EARTH AND SPACE SCIENCES

RESEARCH ARTICLE
10.1029/2024GC011461

Magnetic Hysteresis Properties of Magnetite: Trends With Particle Size and Shape

Greig A. Paterson[1], Roberto Moreno[2,3], Adrian R. Muxworthy[4], Lesleis Nagy[1], Wyn Williams[2], and Lisa Tauxe[5]

[1]Department of Earth, Ocean and Ecological Sciences, University of Liverpool, Liverpool, UK, [2]School of GeoSciences, University of Edinburgh, Edinburgh, UK, [3]Instituto de Física Enrique Gaviola, Ciudad Universitaria, Córdoba, Argentina, [4]Department of Earth Science and Engineering, Imperial College London, London, UK, [5]Scripps Institution of Oceanography, La Jolla, CA, USA

Key Points:

- Magnetic hysteresis is micromagnetically modeled for oblate, prolate and equant magnetite particles (45–195 nm)
- Hysteresis loop shape is highly dependent on particle size/shape due to complex switching behavior of single vortex states
- Transient magnetic hysteresis is a powerful tool for identifying stable remanent magnetizations but is currently infrequently reported

Correspondence to:
G. A. Paterson,
greig.paterson@liverpool.ac.uk

Citation:
Paterson, G. A., Moreno, R., Muxworthy, A. R., Nagy, L., Williams, W., & Tauxe, L. (2024). Magnetic hysteresis properties of magnetite: Trends with particle size and shape. *Geochemistry, Geophysics, Geosystems*, *25*, e2024GC011461. https://doi.org/10.1029/2024GC011461

Received 23 JAN 2024
Accepted 13 AUG 2024

Author Contributions:
Conceptualization: Greig A. Paterson, Roberto Moreno, Adrian R. Muxworthy, Lesleis Nagy, Wyn Williams
Data curation: Greig A. Paterson, Roberto Moreno
Formal analysis: Greig A. Paterson, Roberto Moreno, Adrian R. Muxworthy, Lesleis Nagy, Wyn Williams
Funding acquisition: Greig A. Paterson, Adrian R. Muxworthy, Lesleis Nagy, Wyn Williams, Lisa Tauxe
Methodology: Greig A. Paterson, Roberto Moreno, Wyn Williams
Software: Greig A. Paterson, Wyn Williams
Validation: Roberto Moreno
Visualization: Greig A. Paterson
Writing – original draft: Greig A. Paterson

Abstract Magnetic hysteresis measurements are routinely made in the Earth and planetary sciences to identify geologically meaningful magnetic recorders, and to study variations in present and past environments. Interpreting magnetic hysteresis data in terms of domain state and paleomagnetic stability are major motivations behind undertaking these measurements, but the interpretations remain fraught with challenges and ambiguities. To shed new light on these ambiguities, we have undertaken a systematic micromagnetic study to quantify the magnetic hysteresis behavior of room-temperature magnetite as a function of particle size (45–195 nm; equivalent spherical volume diameter) and shape (oblate, prolate and equant); our models span uniformly magnetized single domain (SD) to non-uniformly magnetized single vortex (SV) states. Within our models the reduced magnetization associated with SV particles marks a clear boundary between SD (≥0.5) and SV (<0.5) magnetite. We further identify particle sizes and shapes with unexpectedly low coercivity and coercivity of remanence. These low coercivity regions correspond to magnetite particles that typically have multiple possible magnetic domain state configurations, which have been previously linked to a zone of unstable magnetic recorders. Of all the hysteresis parameters investigated, transient hysteresis is most sensitive to particles that exhibit such domain state multiplicity. When experimental transient hysteresis is compared to paleointensity behavior, we show that increasing transience corresponds to more curved Arai plots and less accurate paleointensity results. We therefore strongly suggest that transient behavior should be more routinely measured during rock magnetic investigations.

Plain Language Summary Characterizing the magnetic properties and behavior of natural materials in the Earth and planetary sciences is key to identifying reliable magnetic recorders and variations in the environment. One standard method for achieving this is through room-temperature measurements of magnetic hysteresis. However, the interpretation of magnetic hysteresis data remains one of the most challenging aspects of rock magnetism. To improve our understanding of magnetic hysteresis data, we have systematically investigated how the hysteresis properties of distributions of randomly oriented magnetite change as a function of particle size and shape and how this can help us quantify the contents of natural materials and identify rocks that may give unreliable magnetic signals. We model prolate, oblate and equant magnetite particles in the size range 45–195 nm. We show that magnetic hysteresis defines a clear boundary between simple uniform magnetic structures and more complex non-uniform magnetic structures. We also identify the sizes and morphologies of magnetic particles that are likely to have unstable remanent magnetizations. These unstable particles are associated with distinctive hysteresis behavior, suggesting that hysteresis data can be used to identify rock samples dominated by such behavior.

1. Introduction

Due to the relative ease and rapidity of measurement, magnetic hysteresis is a widely used technique in paleo-, rock, and environmental magnetic analysis and underpins assertions around magnetic particle size and paleomagnetic stability (e.g., Day et al., 1977; Dunlop, 2002; Paterson et al., 2017). Despite the ease of measurement, processing and analyzing hysteresis data can be complicated (e.g., Jackson & Solheid, 2010; Paterson et al., 2018), and the ubiquity of hysteresis data can lead to overly simplified or misinterpreted implications of these data when dealing with magnetically complex materials (e.g., Roberts et al., 2018). Recent literature has highlighted the challenges of using hysteresis data for domain state identification (e.g., Roberts et al., 2018);

Writing – review & editing:
Roberto Moreno, Adrian R. Muxworthy, Lesleis Nagy, Wyn Williams, Lisa Tauxe

however, other work has suggested that hysteresis data have utility in quantifying the relative stability of paleomagnetic recorders (e.g., Paterson et al., 2017). Some hysteresis experiments, such as determining First Order Reversal Curves, FORCs (Roberts et al., 1995), are quite time consuming, while others, such as measuring only the outer loops or just the transient hysteresis (Fabian, 2003; Yu & Tauxe, 2005), are fast. Hence, there is a trade-off between in-depth and time consuming measurements to decompose bulk specimen properties and the more rapid quantification of bulk hysteresis behavior and implications for other magnetic properties measured on bulk specimens (e.g., paleomagnetic directions or paleointensities). Nevertheless, in both types of experiments, a comprehensive understanding of particle level hysteresis behavior is required to be able to fully interpret hysteresis data.

Although extensive experimental observations of magnetic hysteresis in sized particles of (nominally) magnetite have been made (e.g., Argyle & Dunlop, 1990; Day et al., 1977; Krása et al., 2009), there are challenges in constraining particle size distributions, maintaining a single mineralogy, as well as preventing magnetostatic interactions between particles. There also remains the unquantified, and highly variable, particle geometry of these synthetic samples, which can play a notable role in their hysteresis properties (Williams et al., 2006).

Williams et al. (2006) and Yu and Tauxe (2008) explored hysteresis in magnetite as a function of particle geometry, where configurational anisotropy has a large or dominant control on the net anisotropy. They both illustrated that angular geometries tend to have higher coercivities due to the "pinning" effect of sharp surface angles. Yu and Tauxe (2008) further explored the influence of particle elongation (i.e., shape anisotropy) for prolate cuboid and octahedral particles that exhibited single vortex (SV) states when equidimensional. As aspect ratio (AR) increases, coercivity (B_c) and remanence ratio (M_{rs}/M_s) initially decrease due to a close balance between magnetocrystalline and shape anisotropy. As AR increases further, above ∼1.2, shape anisotropy dominates and both B_c and M_{rs}/M_s increase. These previous studies are based on low resolution finite difference models, whose domain structures are evident, but the coercivities are far more sensitive to model resolution and edge effects. The characteristic hysteresis signals of isolated particles of varying size, shape, and composition are therefore not comprehensively understood, neither experimentally nor micromagnetically.

In this work, we expanded the micromagnetic approach to systematically map out magnetic hysteresis behavior as a function of size and shape of isolated magnetite particles. Unlike Williams et al. (2006) and Yu and Tauxe (2008), we explore the effects of particle shape at particle sizes up to 195 nm, and include oblate particle shapes, which were not part of the previous works. We evaluate the relative changes of common hysteresis parameters and what these mean in relation to magnetic domain states and magnetic stability of the modeled particles. Before introducing our micromagnetic models, we start with an overview of magnetic hysteresis and the main parameters derived from these data.

2. Hysteresis Measurement and Derived Properties

A hysteresis loop is initiated by saturating a specimen's magnetization in a large field, typically >300 mT for magnetically soft materials or ≫1–10 T for magnetically hard materials (Figure 1a). From the saturated magnetization (M_s) state, the field is gradually reduced to the equivalent negative saturating field and swept back to positive saturation to complete the loop. The magnetization at the zero-field point is known as the saturation remanent magnetization (M_{rs}).

During the initial field sweep, a single domain (SD) magnetic particle will experience a critical switching of its magnetization to negative saturation as the field sweeps through a critical field, known as the coercivity (B_c). Particles too large for a uniformly magnetized SD state have more complex magnetization structures such as single (SV) states (Schabes & Bertram, 1988; Williams & Dunlop, 1989) or multi-vortex (MV) states (Khakhalova et al., 2018; Lascu et al., 2018). Such particles can experience changing domain states with changing fields, and switching of the magnetization may occur as a number of discrete steps caused by nucleation and denucleation of the vortex structures (e.g., Lascu et al., 2018; Williams & Dunlop, 1995).

A number of other properties can be derived from a hysteresis loop by comparing the upper and lower branches (e.g., Fabian, 2003; Rivas et al., 1981). The average and the difference of the upper and lower branches are the induced and remanent hysteretic branches, respectively (Paterson et al., 2018; Rivas et al., 1981; von Dobeneck, 1996). The fields at which these curves fall to half of their peak values represent the median destructive field

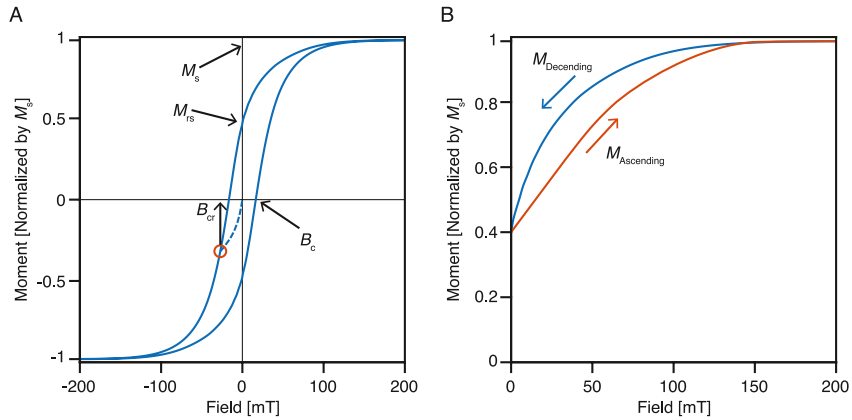

Figure 1. (a) Schematic illustration of a hysteresis loop and associated parameters. The solid blue curve shows a hysteresis loop and the dashed blue curve is the back-field demagnetization curve used to determine the coercivity of remanence (B_{cr}). See text for description of the remaining parameters. (b) Schematic illustration of a transient hysteresis loop whereby the descending loop from saturation is terminated at zero field and the field is then increased back to saturation. The transient hysteresis of Fabian (2003) is twice the area between the two curves, which accounts for the transient behavior in the negative field half of the hysteresis loop.

in the induced and remanent branches B_{ih} and B_{rh}, respectively (Fabian & von Dobeneck, 1997; von Dobeneck, 1996).

Fabian (2003) quantified the shape of a hysteresis loop, σ_{hys}, which is the log of the ratio of the area of the loop to the area of the equivalent square hysteron for the observed M_s and B_c. The shape parameter gives a measure of the "squareness" of a hysteresis loop and is sensitive to bulging or pinching of hysteresis loops at low fields. A σ_{hys} value of zero indicates that the two loops have an equivalent area and hence a similar shape. Positive values are indicative of "wasp-waisted" loops and negative values are indicative of "pot-bellied" loops (Tauxe et al., 1996). Deviations from a σ_{hys} of zero are typically interpreted as being indicative of particle populations with distinct coercivities arising from the mixing of different particle sizes or different mineralogy (e.g., Roberts et al., 1995; Tauxe et al., 1996).

In a typical suite of rock magnetic measurements, additional data are often acquired to characterize the properties of a specimen. One such measurement is the back-field demagnetization curve, also known as a DC demagnetization curve. In a back-field measurement, a specimen is initially in the positive remanent saturation state (M_{rs}). A small negative field is applied then removed and the magnetization is allowed to relax to a remanent state, which should be partially demagnetized with respect to the initial positive remanent saturation state. The negative, or back-field, is progressively decreased until the specimen reaches the negative remanent saturation state. The field at which the remanent magnetization falls to zero is called the coercivity of remanence (B_{cr}). For an isolated SD particle, switching of remanence will occur in a single critical switching at B_{cr}. For non-SD particles, the switching of remanence states can occur in multiple discrete switches linked to changing domain states.

An important point to note is that while for SD particles, B_c and B_{cr} generally represent critical switching fields, and for SV states, B_{cr} is a critical switching field but B_c may not be. That is, application of the B_{cr} field represents an irreversible switch in the magnetization, while the magnetization at B_c may, in some cases, be reversible.

Transient hysteresis, T_{hys} (Figure 1b), which takes a specimen from positive saturation to the saturation remanent state (part of the major hysteresis branch) and then back to the positive saturation state (a minor hysteresis curve), is the area mapped out by difference in these two hysteresis branches (Fabian, 2003; Fabian & von Dobeneck, 1997; Yu & Tauxe, 2005). T_{hys} is quantified as the ratio of twice the transient area (to account for the negative field transient) to the area of the whole hysteresis loop (Fabian, 2003). In a uniformly magnetized SD particle, the field sweep has not passed the critical switching field represented by B_c, so the magnetization from the remanent state back to saturation is completely reversible. Hence, SD particles exhibit zero T_{hys}. In non-SD particles, the progressive switching steps during the field sweep caused by domain states changes in the return from remanence to saturation can be irreversible and result in substantial T_{hys}. In SV domain states, transient hysteresis is caused by vortex nucleation and denucleation occurring at different fields as the field is swept down

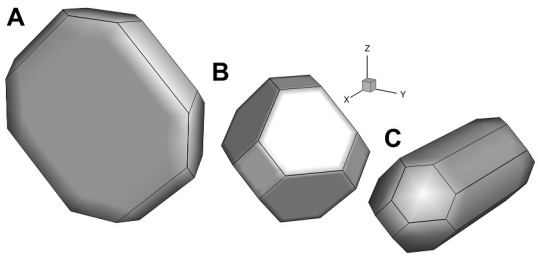

Figure 2. Examples of the range of geometries modeled in this study. Particles with an equivalent spherical volume diameter of 45 nm representing (a) oblate (aspect ratio [AR] = 0.17), (b) equant (AR = 1.00), and (c) prolate (AR = 2.75) geometries.

from saturation and then back up, respectively (Yu & Tauxe, 2005; Zhao et al., 2017). T_{hys} is therefore indicative of complex and field history dependent changes in domain state. Although straightforward and relatively quick to measure, transient hysteresis is not typically measured in most suites of rock magnetic measurements.

3. Methods

In this study, we micromagnetically model hysteresis loops, transient hysteresis loops, and back-field demagnetization curves as a function of particle size and aspect ratio (AR = length/width) for magnetite at room temperature (20°C). The models were generated using the micromagnetic simulation software MERRILL v1.8.6p (Ó Conbhuí et al., 2018; Williams et al., 2024), with truncated-octahedral geometries created using Coreform Trelis 17.1 (LLC, 2017), meshed at a resolution of 8 nm, which is below the exchange length of magnetite (Rave et al., 1998). In total, we model 16 particle sizes between 45 and 195 nm (expressed as the equivalent spherical volume diameter [ESVD]) and ARs between 0.17 (oblate) and 2.75 (prolate) (Figure 2). Prolate geometries were elongated along the ⟨100⟩ axis and oblate geometries were shortened along ⟨100⟩.

The simulated experiments were undertaken in fields between ±200 mT at 1 mT resolution, with hysteresis loops initiated at positive saturation. For hysteresis loops, only the upper branches were simulated, but through rotational symmetry the lower branch can be determined. To represent a random assemblage of identical particles (i.e., a mono-dispersion), all models were run using 29 field directions evenly distributed over an octant of the unit sphere, using a Fibonacci sphere sequence. Final simulation results are the average of these directions.

Transient hysteresis loop models were initiated from the zero field (M_{rs}) step of the major hysteresis loop. The fields were swept back to 200 mT in steps of 1 mT. Back-field demagnetization curves were determined from the first-order reversal curve (FORC) simulations of Nagy et al. (2024), which were similarly simulated at 1 mT resolution. The zero-field steps of the reversal curves initiated at negative fields were taken as the remanence steps of the back-field demagnetization curves (e.g., Heslop, 2005).

Collectively, our hysteresis, transient and back-field models constitute ∼4.8 million micromagnetic solutions representing determinations of domain states under varying applied field conditions. Classifying all of these domain states is not feasible, and we therefore restrict our domain classification to the 6,032 M_{rs} states from the hysteresis loops (16 particle sizes, 13 geometries, and 29 field directions). Each of these micromagnetic solutions was classified by visual inspection. Here, we make a distinction between "domain state," which refers to the configuration of the magnetization vectors (e.g., uniformly magnetized, SD, vs. SV), and "domain state configuration," which we restrict to refer to an oriented domain structure (e.g., a magnetocrystalline easy axis aligned SV vs. a hard aligned SV) or multiple unique domain states in the same grain.

4. Results

4.1. Domain Characterization

From our classification of remanence domain states, we identify four main states: SD (uniformly magnetized, including flower structures), SV, s-shaped structures (SS), and MV. Examples of each of these states are given in Figure 3.

The domain states in our models are predominantly SD and SV, with SS and MV states occurring only in the largest, most oblate particles. The most frequently occurring domain states for each of our size/shape combinations are shown in Figure 4a. For small particles (≲80 nm), all geometries are SD. At high elongations this extends up to ∼120 nm, but for highly oblate particles, the SD region extends up to ∼175–185 nm. SV states prevail above these sizes and SS states occur for large oblate particles (Figure 4a). We note that our models do not include thermal fluctuations, so it is likely that these SS states are meta-stable and are likely to rapidly collapse into a more stable states, which, for these particles, is an SV state. MV states are only observed in a single model of oblate particles (ESVD = 195 nm, AR = 0.250).

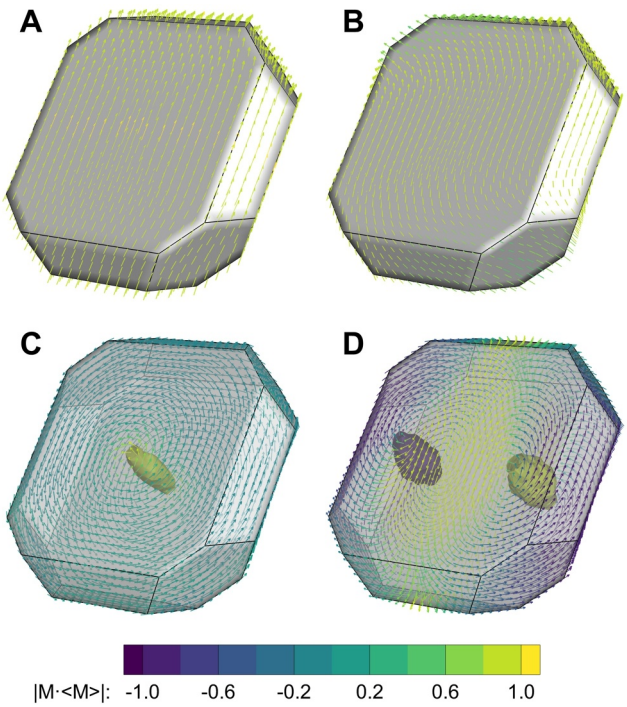

Figure 3. Examples of the main domain states observed in the remanence states of the hysteresis loop. All particles have an aspect ratio of 0.25. (a) A uniformly magnetized single domain state in a 135 nm particle; (b) An s-shaped state in a 155 nm particle; (c) An single vortex state in a 175 nm particle; (d) An multi-vortex state in a 175 nm particle. The magnetization vectors are colored according to the dot product of the individual unit vector and the direction of the particles' net magnetization. In parts (c) and (d), the vortex cores are highlighted by the isosurface of relative helicity at 0.95 (yellow) and −0.95 (purple).

Within the SD region, multiple orientations of magnetization with respect to the magnetic anisotropy are observed; each represents a different domain configuration (Figure 4b). For small particles (≲80 nm) with moderate elongations, the multiple domain configurations correspond to SD states oriented along either a shape or magnetocrystalline anisotropy easy axis. These multiple configurations represent instability in magnetic remanence for particle shapes where these two anisotropy energies are closely balanced (i.e., ARs ∼ 1.2–1.3).

For equant particles (AR of 1), as the particle size increases to ∼85–105 nm, there is a narrow band of particle size that exhibits multiple domain state configurations at remanence. The exception to this is with our 95 nm model, which has multiple domain states (Figure 4b). This narrow size range corresponds to the short relaxation time and low unblocking temperature unstable zone (the "hard aligned" SV state identified by Nagy et al., 2017).

Across all the different particle geometries, the competition between magnetocrystalline or shape anisotropy controlled hard and easy aligned states is responsible for this multiplicity in domain state configurations (Figure 4b). In equant particles, this unstable zone coincides with the transition between SD and SV states, and is a result of the presence of magnetocrystalline hard and easy aligned SV states. For large prolate particles (upper right quadrant of Figure 4b), a large region of domain state configuration multiplicity is observed, with some particles capable of supporting 2–3 different domain configurations. This is similarly the result of both shape hard and easy aligned SV structures. For large oblate particles domain state multiplicity arises from the presence of SV states aligned along a shape hard (short) axis (e.g., Figure 3c) and shape/magnetocrystalline easy aligned SD states.

4.2. Hysteresis Properties

Our simulations exhibit a wide range of behavior characteristic of SD and SV particles (Figure 5); these bear similarity to the range of behavior seen in hysteresis measurements of natural materials (e.g., Nikolaisen et al., 2022; Paterson et al., 2018; Roberts et al., 1995; Wang & Van der Voo, 2004).

From our simulations, we observe a wide range of hysteresis shapes from "wasp-waisted" (Figure 6b) to "pot-bellied" (Figure 6c). There is a strong signal from large oblate particles that have extremely wasp-waisted loops and large prolate particles with pot-bellied loops (Figure 6). In general, however, most particles have negative σ_{hys} indicative of pot-bellied behavior, with the most pot-bellied loops coming from prolate particles (AR ≈ 1.25–

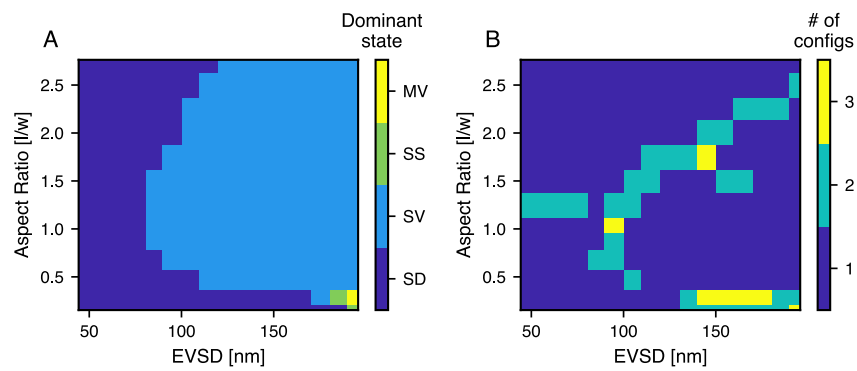

Figure 4. Classification of hysteresis M_{rs} domain states and number of domain state configurations. (a) The most commonly occurring domain state (SD, single domain; SV, single vortex; SS, s-shaped; MV, multi-vortex). (b) The number of unique domain state configurations.

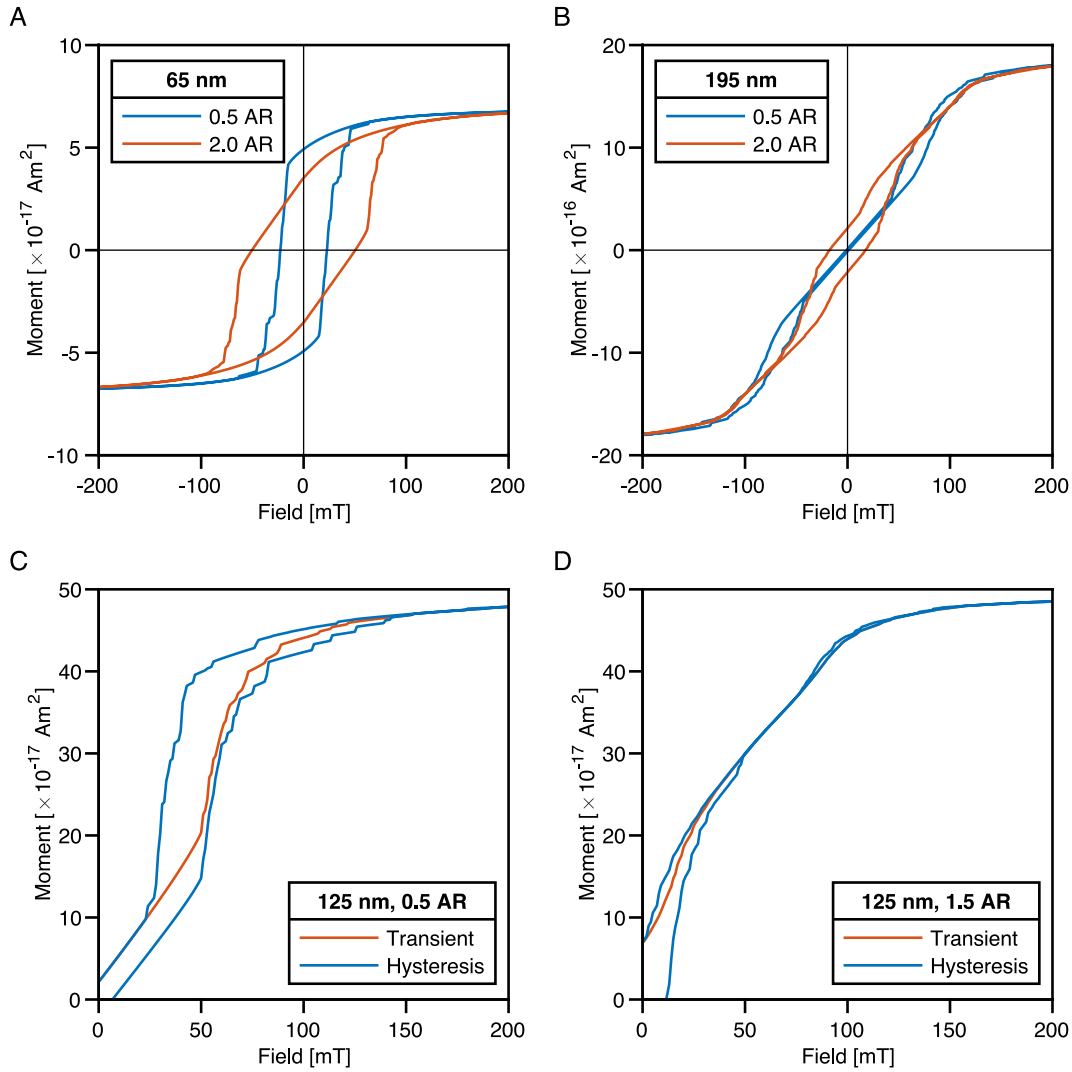

Figure 5. Representative examples of the modeled hysteresis loops for individual particles. (a) Loops from small single domain particles. (b) Loops from large single vortex (SV) dominated particles. Transient loop behavior from SV dominated (c) oblate and (d) prolate particles. For the hysteresis loops, only the upper branch was simulated, but was reflected to create a full hysteresis loop.

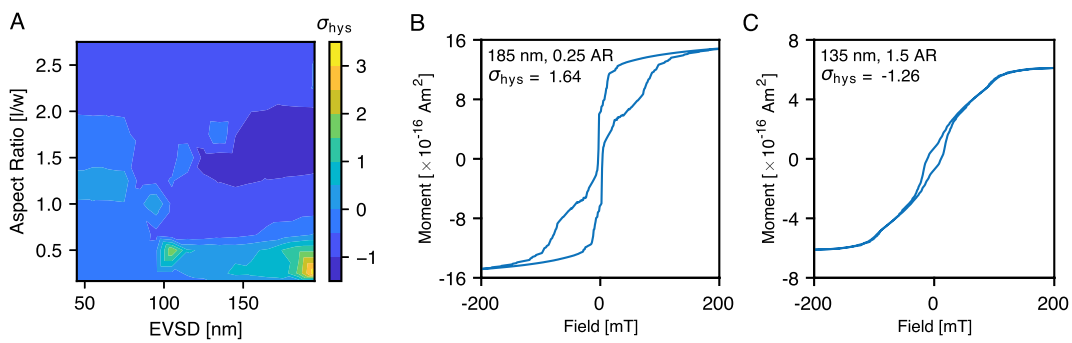

Figure 6. Hysteresis loop shape (σ_{hys}) behavior. (a) Contour map of hysteresis σ_{hys} as function of particle size and aspect ratio. Examples of (b) "wasp-waisted" and (c) "pot-bellied" hysteresis loops.

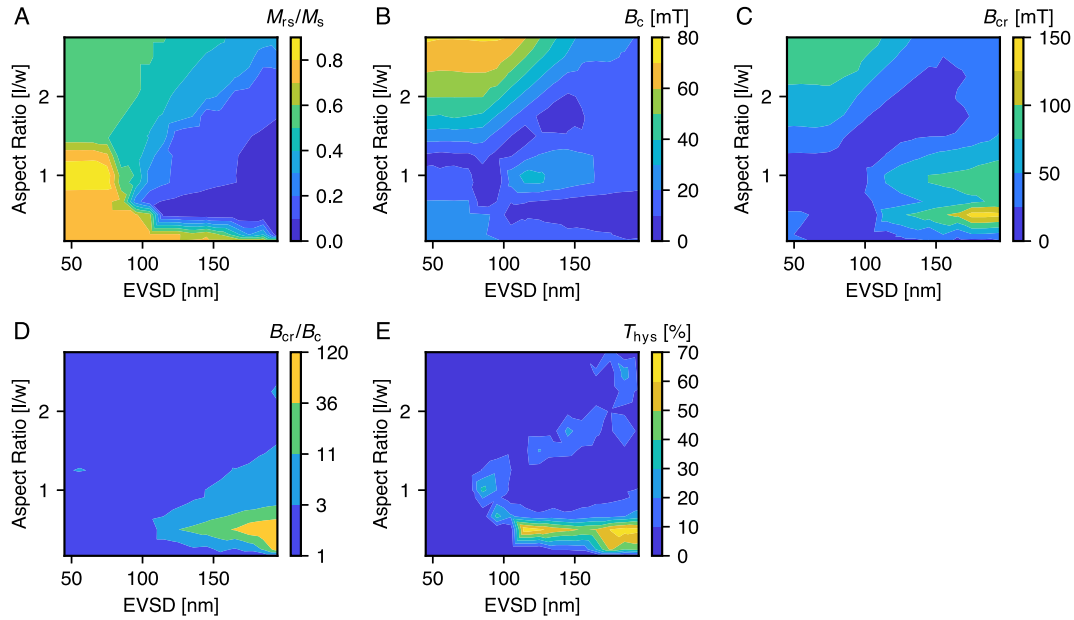

Figure 7. Contour maps of hysteresis properties for random assemblages as a function of particle size and aspect ratio. (a) M_{rs}/M_s, (b) B_c, (c) B_{cr}, (d) B_{cr}/B_c, and (e) Transient hysteresis.

2.00) larger than ≈130 nm (Figure 6a). Wasp-waistedness is predominantly found in small (≲80–90 nm) prolate (AR ∼ 1.25) particles and larger (≳120 nm) oblate particles (AR ≲ 0.5). Despite the range of σ_{hys} observed, the median σ_{hys} of the 208 averaged hysteresis loops is ≈−0.56 (interquartile range of −0.74 to −0.14). This is broadly consistent with the experimental observations of Fabian (2003) using sized powders of synthetic titanomagnetite ($\sigma_{hys} \approx -0.9$ to -0.5).

In Figure 7, we show contour plots of hysteresis parameters as a function of particle size and AR. Transects of these parameters at selected ARs are shown in Figure 8. Small (≲100 nm) oblate, equant, and prolate particles have M_{rs}/M_s values of 0.707, 0.866, and 0.5, respectively (Figure 7a), which are near the expected values for random assemblages of uniformly magnetized particles dominated by biaxial, cubic, and uniaxial magnetocrystalline anisotropy, respectively (Dunlop & Özdemir, 1997; Williams, Moreno, et al., 2024). As the particle size increases, prolate particles exhibit a relatively gradual decrease in M_{rs}/M_s to ∼0.1 at 195 nm, with equant particles experiencing a slightly steeper decrease (Figure 8a). Oblate particles show the largest decrease in M_{rs}/M_s with increasing particle size (Figures 7a and 8a).

The coercivity (B_c) of the models shows that for both the SD and SV states, coercivity increases with increasing AR for prolate particles (Figure 7b). For equant particles of ∼85–95 nm size, there is a dip in the coercivity to values of ∼5 mT, coincident with particles that have short relaxation times (Nagy et al., 2017). This dip in B_c is also seen at all prolate elongations but occurs at larger particle sizes with increasing elongation. For slightly oblate particles, this low coercivity zone exists in ∼85–95 nm particles. Highly oblate particles, however, have consistently low B_c above ∼100 nm, which corresponds to the presence on both SD and SV states in these particles.

Considering B_{cr} (Figure 7c), prolate particles with low B_{cr} values are associated with multiple domain state configurations (Figure 4b) similar to the trend seen for coercivity (Figure 7b). For oblate particles, however, B_{cr} increases with increasing particle size, with the highest values corresponding to particles that have SV structures aligned with a shape hard axis (short axis) in the remanence state. As a result, variations in B_{cr}/B_c are dominated by these states found in oblate particles, which have low B_c and high B_{cr} (Figure 7d). For equant and prolate particles, B_{cr}/B_c remains less than ∼5, but is consistently below 3 for the smallest particles (≲140 nm; Figure 8d).

Transient hysteresis behavior is related to domain states (e.g., vortex states) nucleating at some field as the upper branch sweeps from saturation to zero-field, but denucleating at some higher field as the transient branch sweeps back to saturation (Yu & Tauxe, 2005). Our SD models consistently have transient loop areas (T_{hys}) that are ≪1%

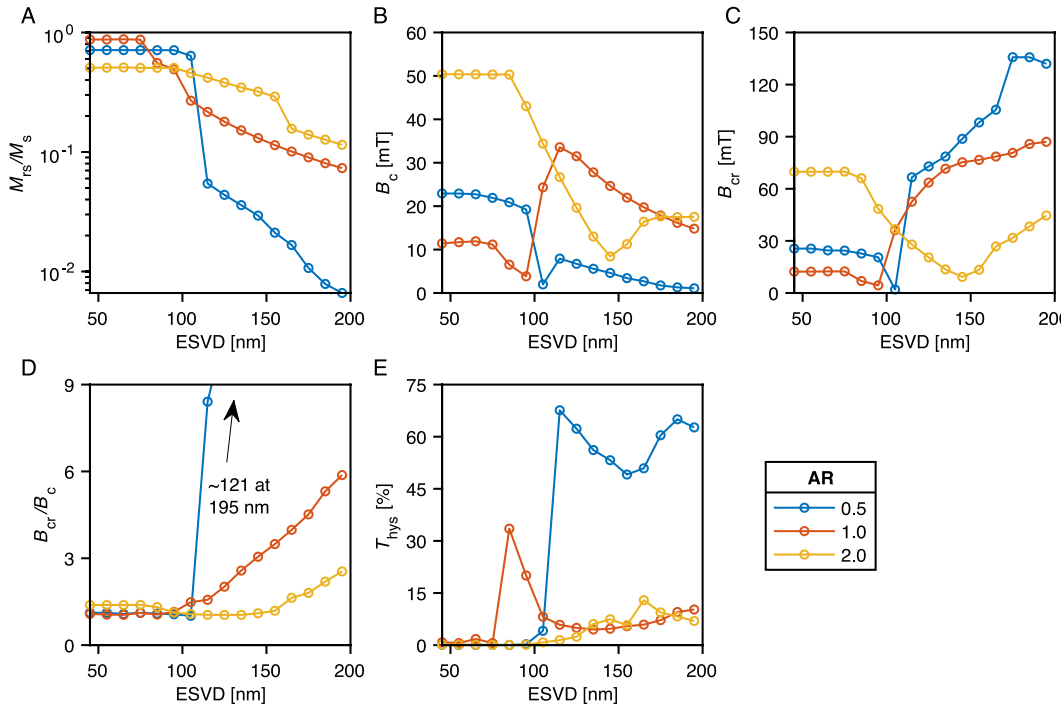

Figure 8. Selected transects through the contour maps shown in Figure 7. (a) M_{rs}/M_s, (b) B_c, (c) B_{cr}, (d) B_{cr}/B_c, and (e) transient hysteresis. The selected aspect ratios are shown in the legend.

of the major loop areas (related to numerical noise and a small degree of flowering), while SV states typically have T_{hys} > 2%–5% (Figure 7e). For a consistent particle geometry, T_{hys} generally increases with increasing particle size (Figure 8e). In equidimensional particles, T_{hys} peaks at 85–95 nm, coincident with the unstable zone in equant magnetite (Nagy et al., 2017). A distinct feature of transient hysteresis behavior is the triangular-like contour region of high T_{hys} (10%–70%; Figure 7e). This arises from oblate particles across a wide range of sizes (~100–195 nm), but the size range varies with particle geometry for prolate particles (e.g., Figures 7e and 8e). Such large T_{hys} behavior is the result of highly variable SV nucleation and denucleation fields and is an indication that the domain state and/or configuration (and hence magnetization) are strongly dependent on the particles' field pre-history.

5. Discussion

5.1. Comparison With Sized Experimental Data

The effectiveness of the micromagnetic approach in predicting the observed domain states from single particle microscopy observations has been well demonstrated (e.g., Almeida et al., 2015, 2016; Khakhalova et al., 2018). Only recently, however, have micromagnetic studies been able to systematically model random assemblages of large (>100 nm) particles (Nikolaisen et al., 2020, 2022).

In Figure 9 we compare our model derived M_{rs}/M_s, B_c, and B_{cr} values with published hysteresis properties from synthetic samples characterized as magnetite with nominal or measured average particle sizes. The aim is not to match exact values but rather compare the range of our simulated results to that of experimental observations. The largest particle we model is 195 nm so the comparison is restricted to experimental data with a reported size <500 nm.

In general, the range of M_{rs}/M_s, B_c, and B_{cr} values from our simulations compares well to those seen in the experimental measurements of sized magnetite particles, which most likely contain distributions of both size and shape (Figure 9). The largest discrepancy is for the oblate particles, where the numerical models predict lower M_{rs}/M_s and B_c values than those seen in the experimental data (Figures 9a and 9b). These low M_{rs}/M_s and B_c values are from oblate particles with ARs of ~0.5–0.67 (Figures 7a and 7b). B_{cr} values show less discrepancy for

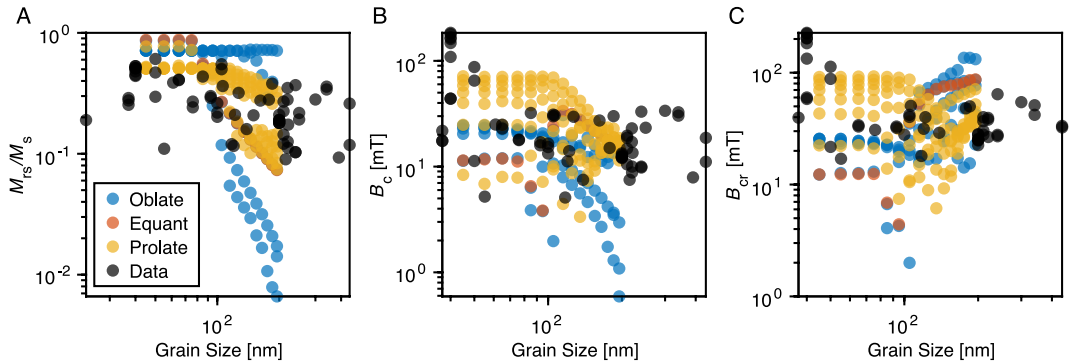

Figure 9. Comparison of model derived hysteresis properties with experimental results from synthetic powders characterized as magnetite with nominal particle sizes. (a) M_{rs}/M_s, (b) B_c, and (c) B_{cr}. Experimental data are for synthetic samples with reported sizes of <500 nm and are taken from Almeida et al. (2015), Argyle and Dunlop (1990), Dunlop (1983, 1986), Krása et al. (2003, 2009, 2011), Levi and Merrill (1978), Muxworthy (1999), Özdemir and Banerjee (1982), Özdemir and O'Reilly (1982), Özdemir et al. (2002), Schmidbauer and Keller (1996), Schmidbauer and Schembera (1987), Smirnov (2009), and Yu et al. (2002).

the oblate particles, but some equant and prolate models have lower B_c values that are not well represented in the experimental data set.

Taking the bounding area mapped out by our simulated results, we can determine the proportion of experimental data that are consistent with our observations (i.e., the percentage of experimental data that lies within the range of our modeled values). This represents the proportion of experimental data (with sizes of 45–195 nm) that could be explained by a linear combination of one or more of our simulations. For M_{rs}/M_s data, ~78% fall with the area bounded by our simulations; for B_c and B_{cr}, this is ~85% ~67%, respectively. This is a good indication that if we mix one or more of our model predictions, it would yield results that are consistent with experimental observations.

5.2. Distinguishing Magnetic Characteristics

A comprehensive discussion of domain state analysis plots (i.e., the Day plot; Day et al., 1977) using our model results, additional micromagnetic simulations, and a more extensive experimental data set are presented in Williams, Moreno, et al. (2024). Here, we restrict the discussion to salient features in whole loop hysteresis data and parameters, discussing the implications for first-order characterization.

In terms of distinguishing the dominant domain state (i.e., SD or SV), M_{rs}/M_s appears to be the most effective parameter: The $M_{rs}/M_s = 0.5$ contour closely follows the SD/SV boundary (Figure 11a) Williams, Moreno, et al. (2024). Out of all sizes and ARs that exhibit only SD and/or SV remanence states (195 our of 208 simulations), only two are predominantly SV with $M_{rs}/M_s \geq 0.5$; the 85 nm particles with ARs of 0.9091 and 1. These particles exhibit only magnetocrystalline hard-axis-aligned vortex states (e.g., Figure 10a), but the vortex core is poorly defined and could also be classified as a twisting flower state (Hertel & Kronmüller, 2002). As a consequence, a larger proportion of magnetization is aligned with the vortex core for these 85 nm particles than expected (cf. a well define SV state Figure 10b). These (near) equant particles fall directly in the unstable zone identified by Nagy et al. (2017) and will have extremely short relaxation times; consequently, due to thermal fluctuations, $M_{rs}/M_s \approx 0$ (i.e., the particles are effectively superparamagnetic, SP).

Differing hysteresis loop shapes (σ_{hys}) are typically attributed to the mixing of different particles with contrasting coercivities as a result of mixed mineralogy (e.g., magnetite and hematite) or mixed particle size (e.g., SP and SD) (Fabian, 2003; Frank & Nowaczyk, 2008; Roberts et al., 1995; Tauxe et al., 1996). Our results, however, are from magnetite mono-dispersions, and do not contain mixed mineralogy or particle sizes. The diversity of loop shapes that we observe (wasp-waisted to pot-bellied) is a result of vortex nucleation/denucleation and/or vortex switching at a range of non-coercivity related fields that are dependent on the field orientation. Although the most extreme shapes are only observed over narrow particle size and geometry ranges, this serves as an important caveat when interpreting hysteresis shape in terms of mixed mineralogy. Similarly, the wide ranging shape values

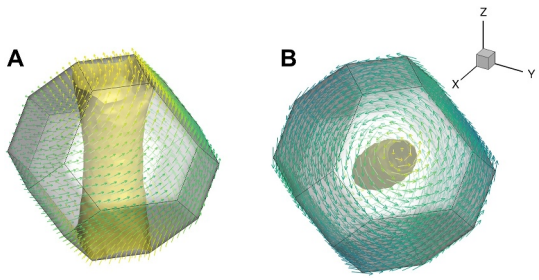

Figure 10. Comparison of single vortex domain states in equant particles. (a) A hard-aligned vortex in a 85 nm particle and (b) an easy-aligned vortex in a 105 nm particle. Colors are the same as in Figure 3.

we observe for SD to SV states means that a similar caution should be considered when interpreting hysteresis loop shape in terms of mixing with SP components.

5.3. Mechanisms of Transient Hysteresis

From our simulations, we observe that transient hysteresis arises from SV states, but not all SV states exhibit transient behavior. Our models show that a large region of SV dominated particles have low T_{hys} (≈2%–5%; Figure 7e). These are typically highly prolate particles that exhibit no transient features in FORC diagrams (Nagy et al., 2024) (e.g., 125 nm with AR = 2.5). In such particles, SV nucleation/denucleation is a near reversible process, which results in near zero transience.

Our models also show that in SV states that do exhibit transient behavior, the magnitude of T_{hys} is shape dependent, with oblate particles typically having larger T_{hys} than prolate particles. This is a result of the difference in the irreversible dynamics of the vortex cores as they respond to the changing field. In prolate particles, large T_{hys} is associated with irreversible SV rotation before denucleation. In oblate particles, however, large T_{hys} is associated with irreversible translation of the vortex core in the oblate plane prior to SV denucleation. In detail, however, these mechanisms are dependent on the field orientation with respect to the particle, with some orientations exhibiting near reversible behavior, hence no to little transience. All of the above described mechanisms and behaviors are illustrated in a series of videos supplementary videos available from Paterson et al. (2024).

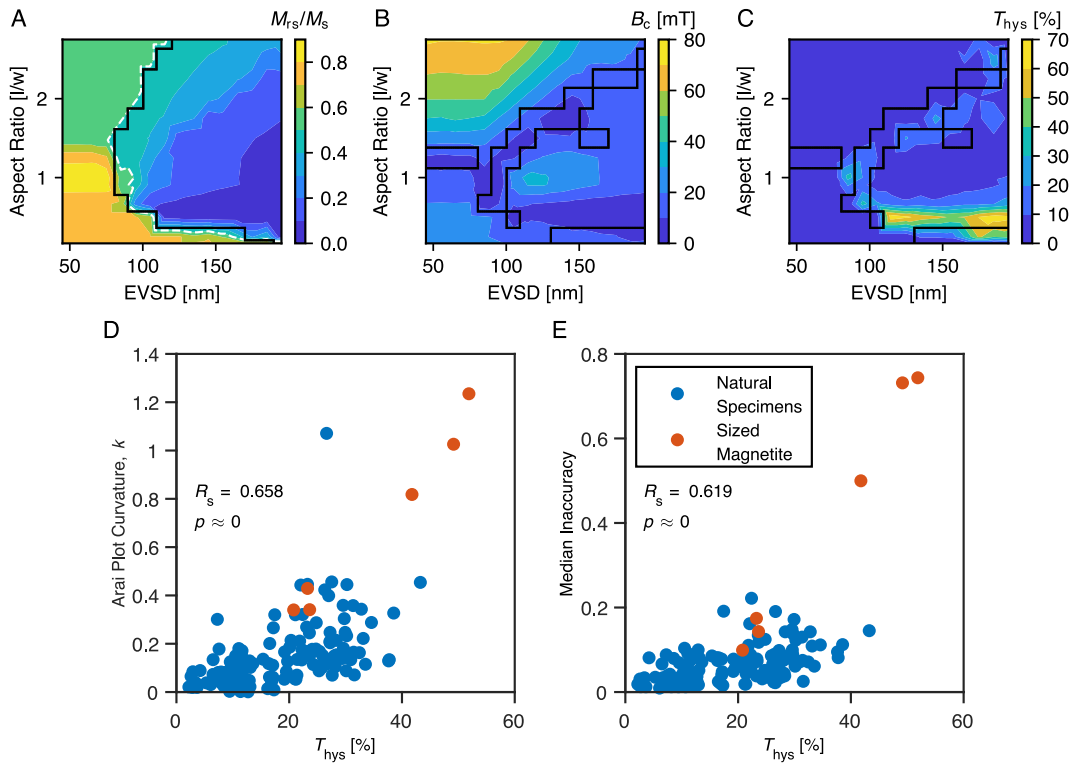

Figure 11. Select contour plots from Figure 7, illustrating (a) M_{rs}/M_s with the $M_{rs}/M_s = 0.5$ contour highlighted by the white dashed line and the single domain/single vortex boundary from Figure 4a given by the black line. (b, c) Are the contour plots of B_c and T_{hys}, respectively, with the region of multiple domain state configurations (Figure 4b) highlighted by the black boxes. Relationship between transient hysteresis (T_{hys}) and (d) curvature of the entire Arai plot and (e) the inaccuracy of the paleointensity fits. R_s is the Spearman rank correlation and p is the associated p-value. The legend in panel (e) also applies to panel (d). Natural specimen data are from Paterson et al. (2017), sized magnetite paleointensity data are from Krása et al. (2003), and T_{hys} data are from Fabian (2003).

5.4. Paleomagnetic Implications

The presence of multiple domain state configurations within a single particle is likely the main cause of unstable paleomagnetic behavior (Cych et al., 2024; Nagy et al., 2017, 2022). In Figures 11b and 11c, we overlay the outline of the size/shape combinations that have multiple domain configurations in the saturation remanence state (derived from Figure 4b) with the contours of B_c/B_c and T_{hys}. This confirms that multiple configurations in monodispersions of magnetite generally correspond to lower B_c (and B_{cr}) and higher T_{hys}.

To further illustrate the potential use of T_{hys} as a proxy for paleomagnetic stability, we replicate the paleointensity analyses of Paterson et al. (2017), comparing paleointensity data (Krása et al., 2003; Paterson et al., 2017) with transient hysteresis (Fabian, 2003; Paterson et al., 2017). Paterson et al. (2017) demonstrated a relationship between the position of a specimen on a Day plot (Day et al., 1977) and the inaccuracy of the paleointensity result as well as the curvature on Arai plots (Paterson, 2011). This data set is smaller than that used by Paterson et al. (2017) as limited T_{hys} are available, but is comprised of 151 natural specimens (described as control specimens in Paterson et al., 2017) and 6 sized magnetite powder specimens (Fabian, 2003; Krása et al., 2003). We calculate the Arai plot curvature from the whole plot and inaccuracy is the median inaccuracy from Paterson et al. (2017) for all Arai plot fits that pass a basic selection process ($n \geq 3, f \geq 0.25, b < 0$, and $g > 0$; see Paterson et al., 2014, for definitions).

In Figures 11d and 11e, we compare the whole Arai plot curvature and median inaccuracy against T_{hys}. This shows positive relationships between transient hysteresis and both paleointensity behaviors, indicating that as T_{hys} increases, both Arai plot curvature and paleointensity inaccuracy become worse. Routine measurement of T_{hys} may therefore help to improve the selection for paleointensity studies or enhance our understanding of the high failure rates of such experiments.

6. Conclusions

In this study, we have undertaken the most comprehensive micromagnetic investigation of magnetic hysteresis in magnetite as a function of particle size and shape to date. The range of behavior we observe is consistent with available experimental observations, giving confidence in the robustness of the simulations.

Our models reveal that hysteresis loops from random assemblages of single sized particles can exhibit varied shapes that result from the variability of vortex nucleation/denucleation and switching depending on the orientation of the field with respect to particle geometry. This is a demonstration that mixed mineralogy or mixed particle sizes are not required to create wasp-waisted to pot-bellied loop shapes.

The particle size and shape range we model predominantly have SD and SV remanence domain states. An M_{rs}/M_s value of 0.5 is the boundary between these states. The SV states observed exhibit both easy- and hard-aligned domain state configurations, with the hard aligned configurations corresponding to the unstable magnetic carriers identified by Nagy et al. (2017).

We have identified distinct particle size and shape combinations that yield low B_c and B_{cr}, indicating low stability particles. These combinations, particularly for B_c, have a correspondence to particles with a higher number of possible domain state configurations (i.e., domain states can be aligned along distinct anisotropy axes), but this relation is less clear for highly prolate particles larger than ∼150 nm.

The area of the transient hysteresis loop, which is rarely measured, has a strong relation to particles that have multiple domain configurations. For transient hysteresis, however, the contrast is more distinct than for B_c and B_{cr}, suggesting that it potentially offers a greater discrimination of behavior likely responsible for unstable paleomagnetic recorders. This inference is supported by a positive relationship between transient hysteresis and both paleointensity inaccuracy and Arai plot curvature. Therefore, we suggest that transient hysteresis should be a routine rock magnetic measurement.

Data Availability Statement

All results reported here were generated using the open source micromagnetic modeling code of Ó Conbhuí et al. (2018). Precompiled versions are available from Williams, Paterson, and Nagy (2024) and the source code for MERRILL is available from Williams et al. (2024) and is provided under a CC-BY-SA 4.0 International

license. All model data presented here and example MERRILL input scripts and Trellis geometry generation scripts to reproduce these models are available from Paterson et al. (2024).

Acknowledgments
G.A.P. acknowledges funding from Natural Environmental Research Council (NERC) Independent Research Fellowship (NE/P017266/1) and Grant NE/W006707/1; W.W. and A.R.M. acknowledge support from NERC Grants NE/S001018/1 and NE/V001388/1. L.N. acknowledges funding from NERC Independent Research Fellowship NE/V014722/1. L.T., W.W. and L.N. acknowledge support of NSFGEO-NERC Grant EAR1827263. L. T., G.A.P., and L.N. acknowledge NSFGEO-NERC Grants EAR1827263 and NE/Y005686/1.

References

Almeida, T. P., Muxworthy, A. R., Kasama, T., Williams, W., Damsgaard, C., Frandsen, C., et al. (2015). Effect of maghemization on the magnetic properties of nonstoichiometric pseudo-single-domain magnetite particles. *Geochemistry, Geophysics, Geosystems*, *16*(9), 2969–2979. https://doi.org/10.1002/2015GC005858

Almeida, T. P., Muxworthy, A. R., Kovács, A., Williams, W., Nagy, L., Conbhuí, P. Ó., et al. (2016). Direct observation of the thermal demagnetization of magnetic vortex structures in nonideal magnetite recorders. *Geophysical Research Letters*, *43*(16), 8426–8434. https://doi.org/10.1002/2016gl070074

Argyle, K. S., & Dunlop, D. J. (1990). Low-temperature and high-temperature hysteresis of small multidomain magnetites (215–540 nm). *Journal of Geophysical Research*, *95*(B5), 7069–7082. https://doi.org/10.1029/JB095iB05p07069

Cych, B., Paterson, G. A., Nagy, L., Williams, W., & Moskowitz, B. (2024). Magnetic domain states and critical sizes in the titanomagnetite series. *Journal of Geophysical Research: Solid Earth*, *129*(6), e2024JB028805. https://doi.org/10.1029/2024JB028805

Day, R., Fuller, M. D., & Schmidt, V. A. (1977). Hysteresis properties of titanomagnetites: Grain-size and compositional dependence. *Physics of the Earth and Planetary Interiors*, *13*(4), 260–267. https://doi.org/10.1016/0031-9201(77)90108-X

Dunlop, D. J. (1983). Viscous magnetization of 0.04 - 100 μm magnetites. *Geophysical Journal of the Royal Astronomical Society*, *74*, 667–687. https://doi.org/10.1111/j.1365-246X.1983.tb01899.x

Dunlop, D. J. (1986). Hysteresis properties of magnetite and their dependence on particle size: A test of pseudo-single-domain remanence models. *Journal of Geophysical Research*, *91*(B9), 9569–9584. https://doi.org/10.1029/JB091iB09p09569

Dunlop, D. J. (2002). Theory and application of the Day plot (M_{rs}/M_s versus H_{cr}/H_c) 1. Theoretical curves and tests using titanomagnetite data. *Journal of Geophysical Research*, *107*(B3), 2056. https://doi.org/10.1029/2001JB000486

Dunlop, D. J., & Özdemir, Ö. (1997). *Rock magnetism: Fundamentals and frontiers* (Vol. 3). Cambridge University Press. https://doi.org/10.1017/cbo9780511612794

Fabian, K. (2003). Some additional parameters to estimate domain state from isothermal magnetization measurements. *Earth and Planetary Science Letters*, *213*(3–4), 337–345. https://doi.org/10.1016/S0012-821X(03)00329-7

Fabian, K., & von Dobeneck, T. (1997). Isothermal magnetization of samples with stable preisach function: A survey of hysteresis, remanence, and rock magnetic parameters. *Journal of Geophysical Research*, *102*(B8), 17659–17677. https://doi.org/10.1029/97JB01051

Frank, U., & Nowaczyk, N. R. (2008). Mineral magnetic properties of artificial samples systematically mixed from haematite and magnetite. *Geophysical Journal International*, *175*(2), 449–461. https://doi.org/10.1111/j.1365-246X.2008.03821.x

Hertel, R., & Kronmüller, H. (2002). Finite element calculations on the single-domain limit of a ferromagnetic cube - A solution to μmag standard problem no. 3. *Journal of Magnetism and Magnetic Materials*, *238*(2), 185–199. https://doi.org/10.1016/S0304-8853(01)00876-9

Heslop, D. (2005). A Monte Carlo investigation of the representation of thermally activated single-domain particles within the day plot. *Studia Geophysica et Geodaetica*, *49*(2), 163–176. https://doi.org/10.1007/s11200-005-0003-70

Jackson, M., & Solheid, P. (2010). On the quantitative analysis and evaluation of magnetic hysteresis data. *Geochemistry, Geophysics, Geosystems*, *11*(4), Q04Z15. https://doi.org/10.1029/2009GC002932

Khakhalova, E., Moskowitz, B. M., Williams, W., Biedermann, A. R., & Solheid, P. (2018). Magnetic vortex states in small octahedral particles of intermediate titanomagnetite. *Geochemistry, Geophysics, Geosystems*, *19*(9), 3071–3083. https://doi.org/10.1029/2018gc007723

Krása, D., Heunemann, C., Leonhardt, R., & Petersen, N. (2003). Experimental procedure to detect multidomain remanence during Thellier-Thellier experiments. *Physics and Chemistry of the Earth*, *28*(16–19), 681–687. https://doi.org/10.1016/S1474-7065(03)00122-0

Krása, D., Muxworthy, A. R., & Williams, W. (2011). Room- and low-temperature magnetic properties of 2-D magnetite particle arrays. *Geophysical Journal International*, *185*(1), 167–180. https://doi.org/10.1111/j.1365-246X.2011.04956.x

Krása, D., Wilkinson, C. D. W., Gadegaard, N., Kong, X., Zhou, H., Roberts, A. P., et al. (2009). Nanofabrication of two-dimensional arrays of magnetite particles for fundamental rock magnetic studies. *Journal of Geophysical Research*, *114*(B2), B02104. https://doi.org/10.1029/2008JB006017

Lascu, I., Einsle, J. F., Ball, M. R., & Harrison, R. J. (2018). The vortex state in geologic materials: A micromagnetic perspective. *Journal of Geophysical Research: Solid Earth*, *123*(9), 7285–7304. https://doi.org/10.1029/2018JB015909

Levi, S., & Merrill, R. T. (1978). Properties of single-domain, pseudo-single-domain, and multidomain magnetite. *Journal of Geophysical Research*, *83*(B1), 309–323. https://doi.org/10.1029/JB083iB01p00309

LLC, C. (2017). Coreform cubit, v16.4 (64-bit). Retrieved from https://coreform.com

Muxworthy, A. R. (1999). Low-temperature susceptibility and hysteresis of magnetite. *Earth and Planetary Science Letters*, *169*(1–2), 51–58. https://doi.org/10.1016/S0012-821X(99)00067-9

Nagy, L., Moreno, R., Muxworthy, A. R., Williams, W., Paterson, G. A., Tauxe, L., & Valdez-Grijalva, M. A. (2024). Micromagnetic determination of the FORC response of paleomagnetically significant magnetite assemblages. *Geochemistry, Geophysics, Geosystems*, *25*(7), e2024GC011465. https://doi.org/10.1029/2024GC011465

Nagy, L., Williams, W., Muxworthy, A. R., Fabian, K., Almeida, T. P., Ó Conbhuí, P., & Shcherbakov, V. P. (2017). Stability of equidimensional pseudo–single-domain magnetite over billion-year timescales. *Proceedings of the National Academy of Sciences of the United States of America*, *114*(39), 10356–10360. https://doi.org/10.1073/pnas.1708344114

Nagy, L., Williams, W., Tauxe, L., & Muxworthy, A. (2022). Chasing tails: Insights from micromagnetic modeling for thermomagnetic recording in non-uniform magnetic structures. *Geophysical Research Letters*, *49*(23), e2022GL101032. https://doi.org/10.1029/2022GL101032

Nikolaisen, E. S., Harrison, R., Fabian, K., Church, N., McEnroe, S. A., Sørensen, B. E., & Tegner, C. (2022). Hysteresis parameters and magnetic anisotropy of silicate-hosted magnetite exsolutions. *Geophysical Journal International*, *229*(3), 1695–1717. https://doi.org/10.1093/gji/ggac007

Nikolaisen, E. S., Harrison, R. J., Fabian, K., & McEnroe, S. A. (2020). Hysteresis of natural magnetite ensembles: Micromagnetics of silicate-hosted magnetite inclusions based on focused-ion-beam nanotomography. *Geochemistry, Geophysics, Geosystems*, *21*(11), e2020GC009389. https://doi.org/10.1029/2020GC009389

Ó Conbhuí, P., Williams, W., Fabian, K., Ridley, P., Nagy, L., & Muxworthy, A. R. (2018). Merrill: Micromagnetic earth related robust interpreted language laboratory. *Geochemistry, Geophysics, Geosystems*, *19*(4), 1080–1106. https://doi.org/10.1002/2017gc007279

Özdemir, Ö., & Banerjee, S. K. (1982). A preliminary magnetic study of soil samples from west-central Minnesota. *Earth and Planetary Science Letters*, *59*(2), 393–403. https://doi.org/10.1016/0012-821X(82)90141-8

Özdemir, Ö., Dunlop, D. J., & Moskowitz, B. M. (2002). Changes in remanence, coercivity and domain state at low temperature in magnetite. *Earth and Planetary Science Letters*, *194*(3–4), 343–358. https://doi.org/10.1016/S0012-821X(01)00562-3

Özdemir, Ö., & O'Reilly, W. (1982). An experimental study of the intensity and stability of thermoremanent magnetization acquired by synthetic monodomain titanomagnetite substituted by aluminium. *Geophysical Journal of the Royal Astronomical Society*, *70*(1), 141–154. https://doi.org/10.1111/j.1365-246X.1982.tb06396.x

Paterson, G. A. (2011). A simple test for the presence of multidomain behavior during paleointensity experiments. *Journal of Geophysical Research*, *116*(B10), B10104. https://doi.org/10.1029/2011JB008369

Paterson, G. A., Moreno Ortega, R., Muxworthy, A. R., Nagy, L., Williams, W., & Tauxe, L. (2024). Micromagnetic hysteresis results for magnetite [Dataset]. *Zenodo*. https://doi.org/10.5281/zenodo.10355841

Paterson, G. A., Muxworthy, A. R., Yamamoto, Y., & Pan, Y. (2017). Bulk magnetic domain stability controls paleointensity fidelity. *Proceedings of the National Academy of Sciences*, *114*(50), 13120–13125. https://doi.org/10.1073/pnas.1714047114

Paterson, G. A., Tauxe, L., Biggin, A. J., Shaar, R., & Jonestrask, L. C. (2014). On improving the selection of Thellier-type paleointensity data. *Geochemistry, Geophysics, Geosystems*, *15*(4), 1180–1192. https://doi.org/10.1002/2013GC005135

Paterson, G. A., Zhao, X., Jackson, M., & Heslop, D. (2018). Measuring, processing, and analyzing hysteresis data. *Geochemistry, Geophysics, Geosystems*, *19*(7), 1925–1945. https://doi.org/10.1029/2018GC007620

Rave, W., Fabian, K., & Hubert, A. (1998). Magnetic states of small cubic particles with uniaxial anisotropy. *Journal of Magnetism and Magnetic Materials*, *190*(3), 332–348. https://doi.org/10.1016/S0304-8853(98)00328-X

Rivas, J., Zamarro, J., Martin, E., & Pereira, C. (1981). Simple approximation for magnetization curves and hysteresis loops. *IEEE Transactions on Magnetics*, *17*(4), 1498–1502. https://doi.org/10.1109/TMAG.1981.1061241

Roberts, A. P., Cui, Y., & Verosub, K. L. (1995). Wasp-waisted hysteresis loops: Mineral magnetic characteristics and discrimination of components in mixed magnetic systems. *Journal of Geophysical Research*, *100*(B9), 17909–17924. https://doi.org/10.1029/95JB00672

Roberts, A. P., Tauxe, L., Heslop, D., Zhao, X., & Jiang, Z. (2018). A critical appraisal of the "Day" diagram. *Journal of Geophysical Research: Solid Earth*, *123*(4), 2618–2644. https://doi.org/10.1002/2017JB015247

Schabes, M. E., & Bertram, H. N. (1988). Magnetization processes in ferromagnetic cubes. *Journal of Applied Physics*, *64*(3), 1347–1357. https://doi.org/10.1063/1.341858

Schmidbauer, E., & Keller, R. (1996). Magnetic properties and rotational hysteresis of Fe_3O_4 and γ-Fe_2O_3 particles ~ 250 nm in diameter. *Journal of Magnetism and Magnetic Materials*, *152*(1–2), 99–108. https://doi.org/10.1016/0304-8853(95)00446-7

Schmidbauer, E., & Schembera, N. (1987). Magnetic hysteresis properties and anhysteretic remanent magnetization of spherical Fe_3O_4 particles in the grain size range 60–160 nm. *Physics of the Earth and Planetary Interiors*, *46*(1–3), 77–83. https://doi.org/10.1016/0031-9201(87)90173-7

Smirnov, A. V. (2009). Grain size dependence of low-temperature remanent magnetization in natural and synthetic magnetite: Experimental study. *Earth Planets and Space*, *61*(1), 119–124. https://doi.org/10.1186/bf03352891

Tauxe, L., Mullender, T. A. T., & Pick, T. (1996). Potbellies, wasp-waists, and superparamagnetism in magnetic hysteresis. *Journal of Geophysical Research*, *101*(B1), 571–583. https://doi.org/10.1029/95JB03041

von Dobeneck, T. (1996). A systematic analysis of natural magnetic mineral assemblages based on modelling hysteresis loops with coercivity-related hyperbolic basis functions. *Geophysical Journal International*, *124*(3), 675–694. https://doi.org/10.1111/j.1365-246X.1996.tb05632.x

Wang, D., & Van der Voo, R. (2004). The hysteresis properties of multidomain magnetite and titanomagnetite/titanomaghemite in mid-ocean ridge basalts. *Earth and Planetary Science Letters*, *220*(1), 175–184. https://doi.org/10.1016/S0012-821X(04)00052-4

Williams, W., & Dunlop, D. J. (1989). Three-dimensional micromagnetic modelling of ferromagnetic domain structure. *Nature*, *337*(6208), 634–637. https://doi.org/10.1038/337634a0

Williams, W., & Dunlop, D. J. (1995). Simulation of magnetic hysteresis in pseudo-single-domain grains of magnetite. *Journal of Geophysical Research*, *100*(B3), 3859–3871. https://doi.org/10.1029/94JB02878

Williams, W., Fabian, K. P. R., Nagy, L., Paterson, G., & Muxworthy, A. R. (2024). Merrill [webpage]. Retrieved from https://bitbucket.org/wynwilliams/merrill

Williams, W., Moreno, R., Muxworthy, A. R., Paterson, G. A., Nagy, L., Tauxe, L., et al. (2024). Vortex magnetic domain state behavior in the day plot. *Geochemistry, Geophysics, Geosystems*, *25*(8), e2024GC011462. https://doi.org/10.1029/2024GC011462

Williams, W., Muxworthy, A. R., & Paterson, G. A. (2006). Configurational anisotropy in single-domain and pseudosingle-domain grains of magnetite. *Journal of Geophysical Research*, *111*(B12), B12S13. https://doi.org/10.1029/2006JB004556

Williams, W., Paterson, G., & Nagy, L. (2024). MERRILL micromagnetic modelling software version 1.8.6. *Zenodo*. https://doi.org/10.5281/zenodo.10556856

Yu, Y., Dunlop, D. J., & Özdemir, Ö. (2002). Partial anhysteretic remanent magnetization in magnetite 1. Additivity. *Journal of Geophysical Research*, *107*(B10), EPM7-1–EPM7-9. https://doi.org/10.1029/2001JB001249

Yu, Y., & Tauxe, L. (2005). On the use of magnetic transient hysteresis in paleomagnetism for granulometry. *Geochemistry, Geophysics, Geosystems*, *6*(1), Q01H14. https://doi.org/10.1029/2004GC000839

Yu, Y., & Tauxe, L. (2008). Micromagnetic models of the effect of particle shape on magnetic hysteresis. *Physics of the Earth and Planetary Interiors*, *169*(1), 92–99. https://doi.org/10.1016/j.pepi.2008.07.006

Zhao, X., Roberts, A. P., Heslop, D., Paterson, G. A., Li, Y., & Li, J. (2017). Magnetic domain state diagnosis using hysteresis reversal curves. *Journal of Geophysical Research: Solid Earth*, *122*(7), 4767–4789. https://doi.org/10.1002/2016JB013683